PHYSICAL REVIEW D **86,** 064039 (2012)

Quasinormal modes of the Bardeen black hole: Scalar perturbations

Sharmanthie Fernando* and Juan Correa†

Department of Physics & Geology, Northern Kentucky University, Highland Heights, Kentucky 41099, USA

(Received 12 July 2012; published 25 September 2012)

The purpose of this paper is to study quasinormal modes (QNM) of the Bardeen black hole due to scalar perturbations. We have done a thorough analysis of the QNM frequencies by varying the charge q, mass M and the spherical harmonic index l. The unstable null geodesics are used to compute the QNM's in the eikonal limit. Furthermore, massive scalar field modes are also studied by varying the mass of the field. Comparisons are done with the QNM frequencies of the Reissner-Nordstrom black hole.

DOI: 10.1103/PhysRevD.86.064039 PACS numbers: 04.70.Bw

I. INTRODUCTION

In general, black hole space-times are expected to have horizons as well as singularities covered by the horizons. Contrary to this notion, a ''regular'' space-time without a singularity and with a horizon was proposed by Bardeen [1]. This particular paper is not readily available. However, a discussion of this model is given by Borde in Refs. [2,3]. There were other regular black holes other than the one proposed by Bardeen and they were all referred to as ''Bardeen black holes'' by Borde [2]. In this paper, we will focus on the space-time proposed by Bardeen [1].

Ayón-Beato and García [4] proposed a model of nonlinear electrodynamics coupled to Einstein gravity to obtain a Bardeen black hole as an exact solution. Hence, the Bardeen black hole can be interpreted as the solution to a nonlinear magnetic monopole with a mass M and a charge q [4]. Ayón-Beato and García [4] have presented several other interesting regular solutions with nonlinear electrodynamics coupled to General Relativity in Refs. [5–8].

There are several works in the literature related to the Bardeen black hole. Gravitational lensing of the regular black hole was studied by Eiroa and Sendra [9]. The geodesic structure of the test particles around the Bardeen black hole was studied by Zhou *et al.* [10]. Gravitational and electromagnetic stability were discussed by Moreno and Sarbach [11]. Quantum corrections for the Bardeen black hole was presented by Sharif and Javed [12].

In this paper, our focus is on studying the scalar field perturbations of the Bardeen black hole and to compute the quasinormal modes of the perturbations.

When a black hole undergoes perturbations, the resulting behavior can be described in three stages. The first stage corresponds to radiation due to the initial conditions of the perturbations. The second stage corresponds to damped oscillations with complex frequencies. These frequencies are independent of the initial conditions and are only dependent on the black hole properties such as the mass, charge and the angular momentum. These modes are called quasinormal modes (QNM). The third stage in general corresponds to a power law decay of the fields.

QNM's have attracted lot of attention from the research community. First of all, there is interest from the experimental point of view, since, there is hope that the QNM's may be detected by the gravitational antennas such as LIGO, VIRGO and LISA in the future. Since the QNM's only depend on the properties of the black holes, such detections would give clues to identify the physical properties of the black holes. On the other hand, due to the famous relation between AdS/CFT duality, many works have focused on studying QNM's of black holes with a negative cosmological constant [13]. Another reason to create interest on QNM's was the conjecture by Hod [14] relating quantum properties of a Schwarzschild black hole and asymptotic QNM's. There are many works aimed at computing asymptotic QNM frequencies along those lines. An excellent review on QNM's is written by Konoplya and Zhidenko [15]. It is fascinating to see some new work relating QNM to various aspects of black hole physics. For example, some recent works have addressed relation between QNM's and hidden conformal symmetry [16,17]. Another interesting paper was written on the connection between gravitational lensing and QNM's by Stefanov *et al.* [18]. Not only black holes, even the naked singularities have been studied from the QNM point of view [19]. Given all the above, it is worthwhile to seek answers how nonlinear sources modify the QNM properties of a black hole.

The paper is presented as follows: In Sec. II, the Bardeen black hole solutions are introduced. In Sec. III, the perturbations by a massless scalar filed is given. In Sec. IV, we will compute the QNM's using the sixth-order WKB approach and discuss the results. In Sec. V, a relation between the null geodesics and the QNM's are presented. In Sec. VI, the perturbations by a massive scalar field is studied. The summary is given in Sec. VII. Directions for further studies are given in Sec. VIII.

II. INTRODUCTION TO THE REGULAR BARDEEN BLACK HOLE

In this section, we will give an introduction to the regular static-charged black hole named the Bardeen black

*fernando@nku.edu
†correaj1@mymail.nku.edu

hole [1]. Ayón-Beato and García [4] interpreted the Bardeen black hole as the gravitational field of a magnetic monopole arising from nonlinear electrodynamics. The proposed action to include the nonlinear electrodynamic term is

$$S = \int d^4x\sqrt{-g}\left[\frac{R}{16\pi G} - \frac{1}{4\pi}\mathcal{L}(F)\right]. \quad (1)$$

Here, R is the scalar curvature, and $\mathcal{L}(F)$ is a function of $F = \frac{1}{4}F_{\mu\nu}F^{\mu\nu}$. Here, $F_{\mu\nu} = 2(\nabla_\mu A_\nu - \nabla_\nu A_\mu)$ is the electromagnetic field strength. In Ref. [4] the authors derived the function $\mathcal{L}(F)$ in order to obtain the Bardeen black hole as

$$\mathcal{L}(F) = \frac{3}{2sq^2}\left(\frac{\sqrt{2q^2F}}{1+\sqrt{2q^2F}}\right)^{\frac{5}{2}}. \quad (2)$$

Here, q and M are the magnetic charge and the mass of the magnetic monopole. Also, $s = \frac{|q|}{2M}$. The equations of motion derived from the action in Eq. (1) are given by

$$G^\nu_\mu = 2\left(\frac{\partial\mathcal{L}}{\partial F}F_{\mu\lambda}F^{\nu\lambda} - \delta^\nu_\mu\mathcal{L}\right), \quad (3)$$

$$\nabla_\mu\left(\frac{\partial\mathcal{L}}{\partial F}F^{\nu\mu}\right) = 0. \quad (4)$$

Static spherically symmetric solution for the above equations were proved to be the Bardeen black hole solution given by the metric

$$ds^2 = -f(r)dt^2 + f(r)^{-1}dr^2 + r^2(d\theta^2 + \sin^2(\theta)d\varphi^2), \quad (5)$$

where

$$f(r) = 1 - \frac{2Mr^2}{(r^2+q^2)^{3/2}}. \quad (6)$$

The magnetic field is given by

$$F_{\theta\varphi} = 2q\sin\theta. \quad (7)$$

For $q \neq 0$, the space-time in Eq. (5) has horizons only if $|q| \leq \frac{4M}{3\sqrt{3}}$. This was shown by Borde [2,3]. For $q > \frac{4M}{3\sqrt{3}}$, there are no horizons. For $q = \frac{4M}{3\sqrt{3}}$, there are degenerate horizons. The function $f(r)$ is plotted in Fig. 1 for varying magnetic charge q.

Asymptotically, the metric function $f(r)$ behaves as

$$f(r) \approx 1 - \frac{2M}{r} + \frac{3Mq^2}{r^3} + O\left(\frac{1}{r^5}\right). \quad (8)$$

The metric for the black hole in Einstein-Maxwell gravity, given by the well-known Reissner-Nordstrom black hole, with a magnetic charge is

$$ds^2 = -f(r)_{\mathrm{RN}}dt^2 + f(r)^{-1}_{\mathrm{RN}}dr^2 + r^2(d\theta^2 + \sin^2(\theta)d\varphi^2), \quad (9)$$

where

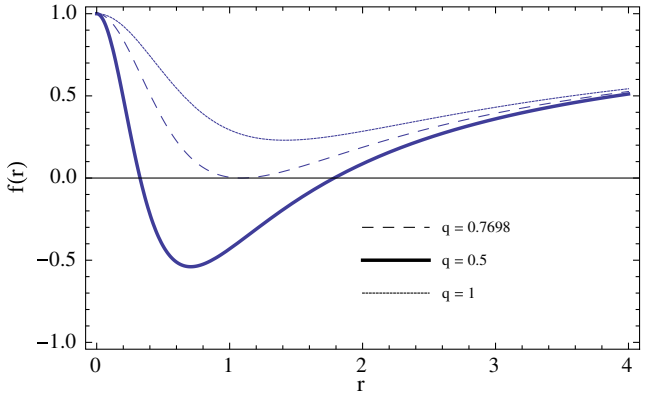

FIG. 1 (color online). The figure shows the function $f(r)$ for $M = 1$ and varying values of q.

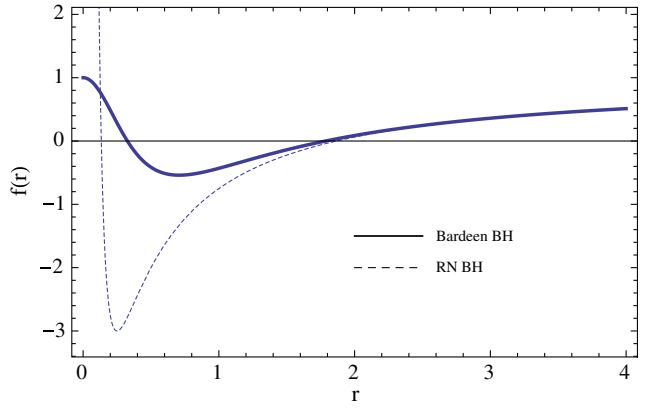

FIG. 2 (color online). The figure shows the function $f(r)$ for the Bardeen black hole (dark line) and the Reissner-Nordstrom black hole (dashed line). Here, $M = 1$ and $q = 0.5$.

$$f(r)_{\mathrm{RN}} = 1 - \frac{2M}{r} + \frac{q^2}{r^2}. \quad (10)$$

In Fig. 2, the two metric functions for the Bardeen black hole and the Reissner-Nordstrom black hole are plotted for comparison. It is clear from Fig. 2, that both black holes have two horizons. For small r, the behavior is somewhat different even though asymptotically both functions are similar. The nonsingular nature of the function $f(r)$ for the Bardeen black hole is observed from Fig. 2. As discussed in Ref. [4], the space-time is regular everywhere since all the scalar curvatures, R, $R_{\mu\nu}R^{\mu\nu}$ and $R_{\mu\nu\alpha\beta}R^{\mu\nu\alpha\beta}$ are regular everywhere. However, the electromagnetic invariant $F = \frac{q^2}{2r^4}$ has singular behavior. The Bardeen black hole satisfies the weak-energy condition.

The Hawking temperature of the Bardeen black hole is given by

$$T = -\frac{1}{4\pi}\frac{dg_{tt}}{dr}\bigg|_{r=r+} = \frac{1}{4\pi}\left[\frac{2Mr_+(r_+^2 - 2q^2)}{(q^2+r_+^2)^{5/2})}\right]. \quad (11)$$

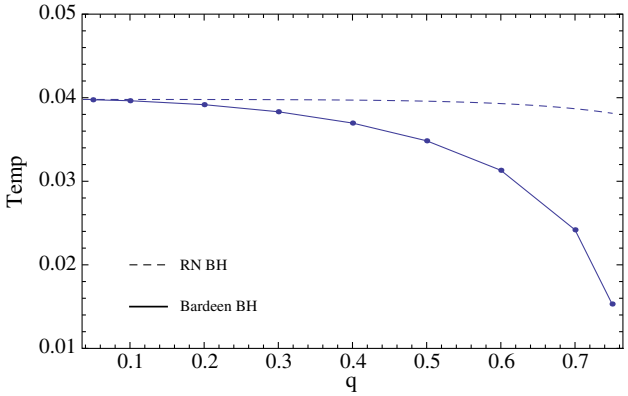

FIG. 3 (color online). The figure shows the temperature T for the Bardeen black hole (dark line) and the Reissner-Nordstrom black hole (dashed line) as a function of the magnetic charge q. Here, $M = 1$.

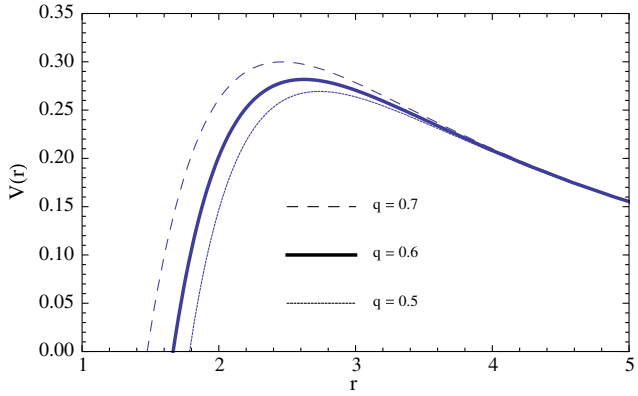

FIG. 4 (color online). The behavior of the effective potential $V(r)$ with the charge for the Bardeen black hole. Here, $M = 1$ and $l = 2$. The height of the potential decreases when the charge decreases.

Here, r_+ is the event horizon of the black hole which is a solution of $f(r) = 0$. In comparison, the Hawking temperature for the Reissner-Nordstrom black hole is

$$T_{\mathrm{RN}} = \frac{1}{4\pi}\left[\frac{2M}{r_+^2} - \frac{2q^2}{r_+^3}\right]. \tag{12}$$

The temperature for both black holes for the same mass is plotted in Fig. 3. The Reissner-Nordstrom black hole is "hotter" than the Bardeen black hole.

III. MASSLESSS SCALAR PERTURBATION OF BARDEEN BLACK HOLES

In this section, we will introduce scalar perturbation by a massless field around the Bardeen black hole. The Klein-Gordon equation for a massless scalar field Φ in curved space-time can be written as

$$\nabla^2 \Phi = 0, \tag{13}$$

which is equal to

$$\frac{1}{\sqrt{-g}}\partial_\mu(\sqrt{-g}g^{\mu\nu}\partial_\nu\Phi) = 0. \tag{14}$$

Using the ansatz for the scalar field Φ,

$$\Phi = e^{-i\omega t}Y(\theta, \phi)\frac{\xi(r)}{r}. \tag{15}$$

Equation (14) simplifies to the Schrödinger-type equation given by

$$\frac{d^2\xi(r)}{dr_*^2} + (\omega^2 - V(r_*))\xi(r) = 0, \tag{16}$$

where

$$V(r) = \frac{l(l+1)f(r)}{r^2} + \frac{f(r)f'(r)}{r}. \tag{17}$$

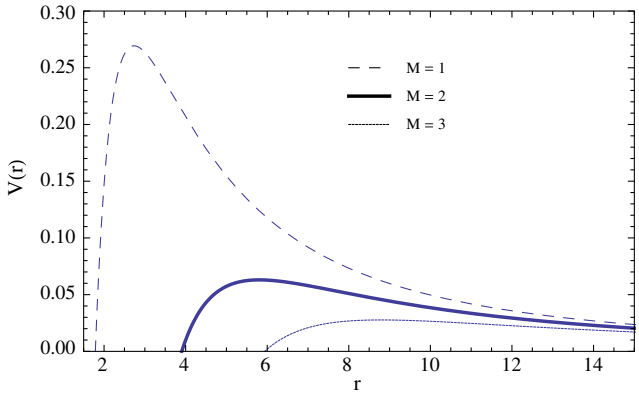

FIG. 5 (color online). The behavior of the effective potential $V(r)$ with the mass M. Here, $q = 0.5$ and $l = 2$. The maximum height of the potential increases as M decreases.

Here, r_* is the well-known "tortoise" coordinate given by

$$dr_* = \frac{dr}{f(r)}. \tag{18}$$

Note that l is the spherical harmonic index. Here, r_* cannot be evaluated explicitly due to the nature of the function $f(r)$. When $r \to \infty$, $r_* \to \infty$ and when $r \to r_+$, $r_* \to -\infty$.

The effective potential $V(r)$ for the Bardeen black hole is plotted to display how it changes with charge q, the mass M, and the spherical harmonic index l in Fig. 4–6, respectively.

We have also plotted the scalar effective potential for the Reissner-Nordstrom black hole with the one for the Bardeen black hole in Fig. 7 for comparison.

A. Remarks on the stability of the black hole

The potentials are real and positive outside the event horizon for all the figures. Hence, following the arguments by Chandrasekhar [20] the Bardeen black holes can be

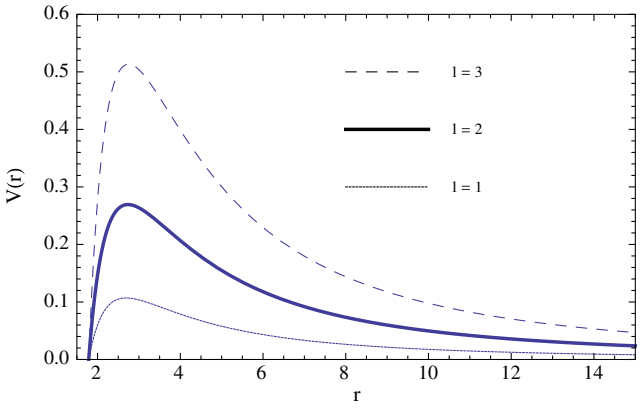

FIG. 6 (color online). The behavior of the effective potential $V(r)$ with the spherical harmonic index l. Here, $M = 1$ and $q = 0.5$. The height of the potential increases when l increases.

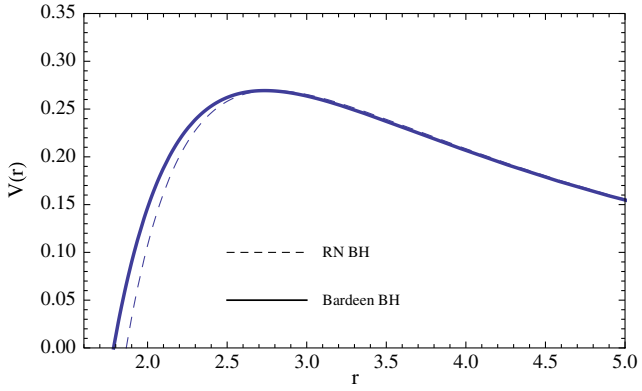

FIG. 7 (color online). The behavior of the effective potential $V(r)$ for the Bardeen black hole (dark line) in comparison with the potential for the Reissner-Nordstrom black hole (dashed line). Here, $M = 1$, $q = 0.2$ and $l = 2$. The potential for the Bardeen black hole is slightly higher in the small r range.

considered stable classically under perturbations by a massless scalar field.

IV. QUASINORMAL MODES OF BARDEEN BLACK HOLE

Quasinormal modes (QNM) for perturbed black hole space-times are the solutions to the wave equation given in Eq. (16). In order to obtain solutions, one has to impose boundary conditions. At the horizons, the boundary condition is such that the wave has to be purely ingoing. In asymptotically flat space-times, such as the Bardeen space-time, the second boundary condition is for the solution to be purely outgoing at spatial infinity.

Usually, the wave equation for black hole perturbations cannot be solved exactly. There are few cases of exactly solved models known to the authors which are mentioned here. In $2 + 1$ dimensions, the wave equations of the well-known BTZ black hole [21], the charged dilaton black hole [22,23], the Lifshitz black hole [24] and the Godel black hole [25] have been solved to obtain exact QNM values. In two dimensions, an asymptotically anti-de-Sitter black hole has been solved exactly [26]. In five dimensions, Nunez and Starinets have obtained exact values for vector perturbations [27].

There are many methods developed to compute QNM's in the literature. In this paper, a semianalytical technique developed by Iyer and Will [28] is followed. The method is based on the WKB approximation. Iyer and Will developed it up to third order and later, Konoplya developed it up to sixth order [29]. Konoplya computed QNM frequencies of D-dimensional Schwarzschild black holes in that paper which also includes a comparison WKB method with varying orders. Examples of the application of the third-order WKB to compute QNM' are given in Refs. [30,31] and of the sixth-order WKB is given in Ref. [32].

We will follow the formalism presented in the paper by Konoplya [29]. In the WKB formula, the QNM frequencies are related to the effective potential in Eq. (17) as

$$\frac{\omega^2 - V_0}{\sqrt{-2V_0''}} - L_2 - L_3 - L_4 - L_5 - L_6 = n + \frac{1}{2}. \quad (19)$$

Here, V_0 and V_0'' are the maximum potential and the second derivative of the potential where the maximum occurs. The expressions for L_2 and L_3 are given in Ref. [28] and L_3, L_4, L_5 and L_6 are given in Ref. [29]. Here, n is the overtone number. The computed ω values are complex and are as $\omega = \omega_R - i\omega_I$.

First, we have computed QNM frequencies by varying the charge of the black hole. We have also computed the QNM's for the Reissner-Nordstrom black hole with the same mass and the charge in order to compare. Here, $n = 0$.

q	ω_R (RN BH)	ω_I (RN BH)	ω_R (Bardeen BH)	ω_I (Bardeen BH)
0.1	0.484455	0.0968185	0.484470	0.0966541
0.2	0.486929	0.0969738	0.486999	0.0963019
0.3	0.491179	0.0972258	0.491380	0.0956563
0.4	0.497411	0.0975605	0.497895	0.0946064
0.5	0.505966	0.0979492	0.507037	0.0929337
0.6	0.517386	0.0983318	0.519668	0.0901727
0.7	0.532561	0.0985743	0.537388	0.0851340
0.76	0.544071	0.0985311	0.551623	0.0796005
0.8	0.553052	0.0983443	**	**
0.85	0.566148	0.0977987	**	**

From Figs. 8 and 9, it is clear that real value of the QNM frequency ω increases when q increases for both black holes. However, the imaginary part of ω decreases for a Bardeen black hole with charge, while for the Reissner-Nordstrom black hole, there is a maximum before it starts

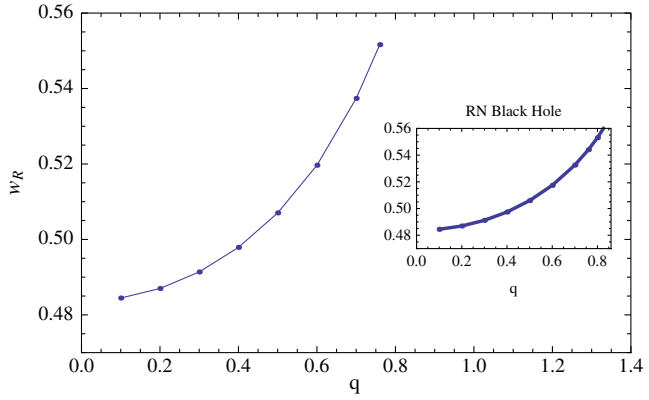

FIG. 8 (color online). The behavior of Re ω with the magnetic charge q for $M = 1$, and $l = 2$.

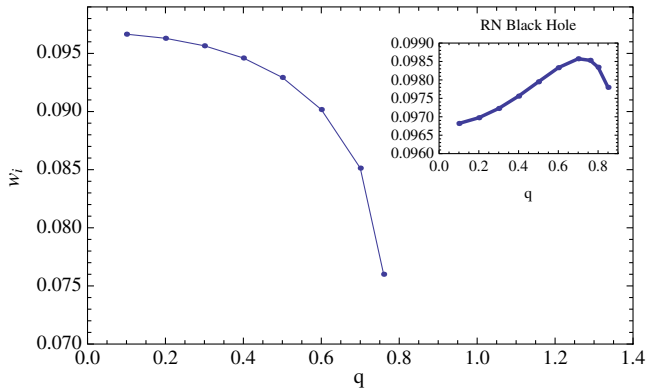

FIG. 9 (color online). The behavior of Im ω with the magnetic charge q for $M = 1$, and $l = 2$.

to decrease. We like to mention here that QNM frequencies for Reissner-Nordstrom black hole were studied by Anderson [33] and Leaver [34]. There is a discussion on some of the earlier work on this subject by Frolov and Novikov [35].

Next, the QNM values are computed for the Bardeen black hole for various values of the mass M as shown in Figs. 10 and 11. Here, $n = 0$.

M	ω_R	ω_I
1	0.5070370	0.0929337
2	0.2444720	0.0480105
3	0.1619870	0.0321495
4	0.1212350	0.0241475
5	0.0968939	0.0193308
6	0.0807027	0.0161148
7	0.0691519	0.0138156
8	0.0604955	0.0120903

When mass M is increases, both ω_R and ω_I decrease.

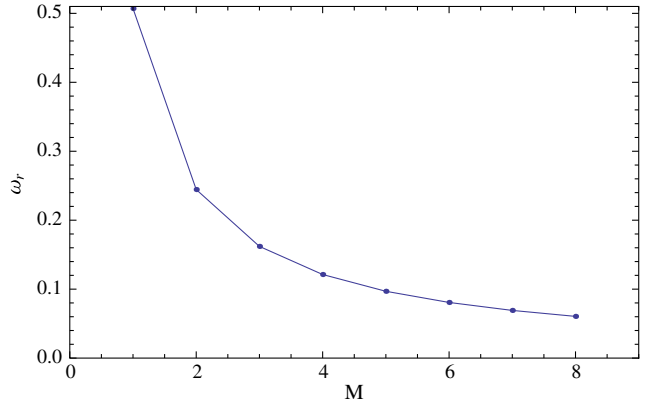

FIG. 10 (color online). The behavior of Re ω with the mass M for $l = 2$, and $q = 0.5$.

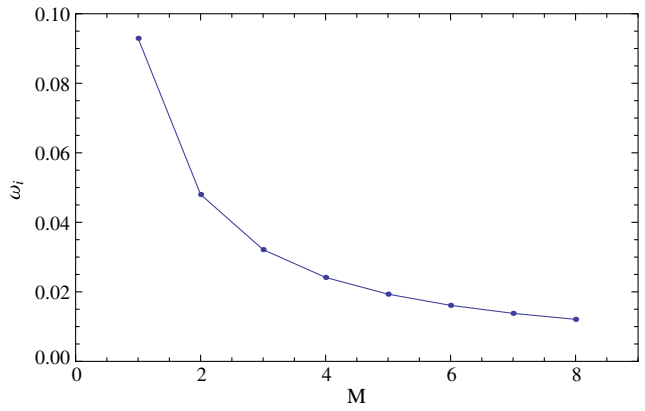

FIG. 11 (color online). The behavior of Im ω with the mass M for $l = 2$, and $q = 0.5$.

Next, the QNM values are computed for the Bardeen black hole for various values of the spherical harmonic index l as shown in Figs. 12–15. Note that the WKB work only for $l > n$. Hence, we have chosen $l = 2$ and computed ω of the fundamental mode with $n = 0$ and the first overtone with $n = 1$.

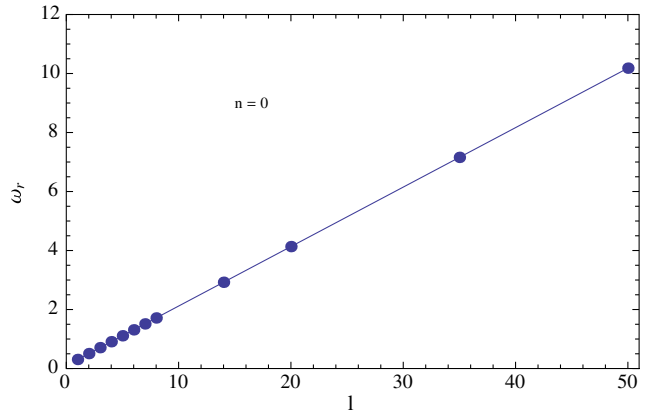

FIG. 12 (color online). The behavior of Re ω with the spherical harmonic index l for $M = 1$, and $q = 0.5$. Here, $n = 0$.

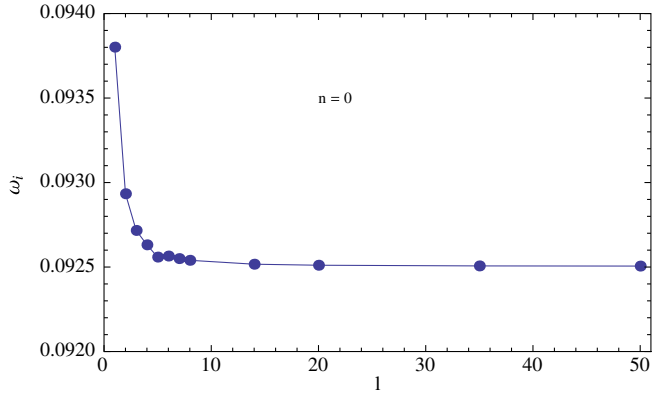

FIG. 13 (color online). The behavior of Im ω with the spherical harmonic index l for $M = 1$, and $q = 0.5$. Here, $n = 0$.

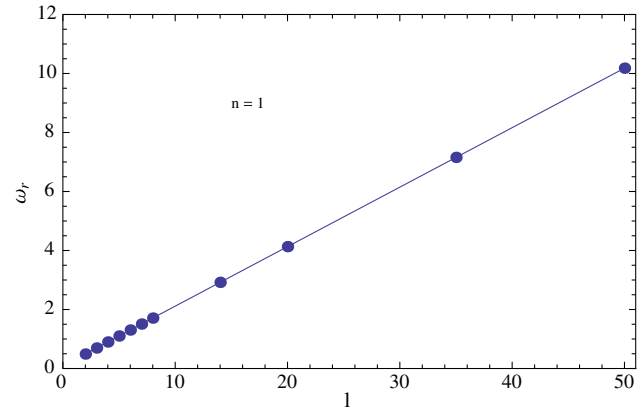

FIG. 14 (color online). The behavior of Re ω with the spherical harmonic index l for $M = 1$, and $q = 0.5$. Here, $n = 1$.

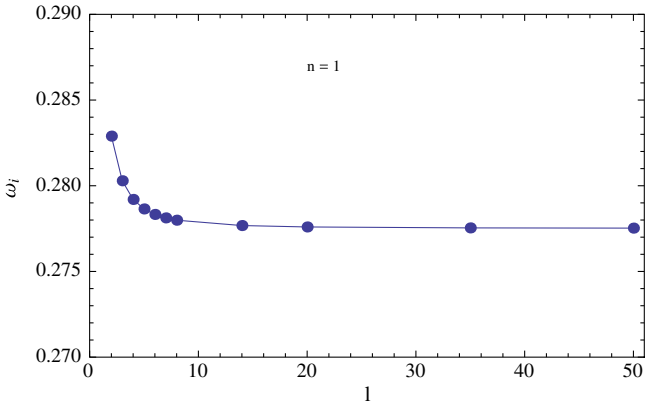

FIG. 15 (color online). The behavior of Im ω with the spherical harmonic index l for $M = 1$, and $q = 0.5$. Here, $n = 1$.

For both $n = 0$ and $n = 1$, ω_R increases linearly with l. On the other hand, ω_I decreases and becomes stable for large l.

V. QNM'S OF THE MASSLESS BLACK HOLES IN THE EIKONAL LIMIT FROM THE NULL GEODESICS OF THE BLACK HOLE

A. ω to the lowest order via null geodesics

Cardoso *et al.* [36] presented an important result to compute the QNM frequencies at the eikonal limit via the unstable null geodesics of the black hole for asymptotically flat black holes. This method was based on some earlier work done along these lines by Mashhon *et al.* [37,38]. This approach has been applied to the Kerr black hole by Dolan [39], the near extreme Kerr black hole by Hod [40] and to the black holes in anti-de-Sitter space by Morgan *et al.* [41].

First, let us give an introduction to the null geodesics of the Bardeen black hole. The geodesics of the Bardeen black hole were studied in detail by Zhou *et al.* [10]. Hence referring to further details to that paper, we will only present the final equation of motion of the photons as

$$\dot{r}^2 + V_{\text{null}} = E^2, \tag{20}$$

with

$$V_{\text{null}} = \left(\frac{L^2}{r^2}\right) f(r). \tag{21}$$

Here, L is the angular momentum of the photons. For $r = r_h$, $V_{\text{null}} = 0$ and for $r \to \infty$, $V_{\text{null}} \to 0$. In Fig. 16, the V_{null} is given for various values of the magnetic charge q. The height is higher for higher charge q.

Referring to the effective potential for the massless scalar field V_{scalar} in Eq. (17), one can see that in the eikonal limit ($l \to \infty$),

$$V_{\text{scalar}} \approx \frac{f(r)l}{r^2}. \tag{22}$$

Hence, one can conclude that the maximum of V_{scalar} occurs at $r = r_m$ given by

$$2f(r_m) - r_m f'(r_m) = 0. \tag{23}$$

Since the effective potential for the null geodesics is given by $V_{\text{null}} = \frac{L^2 f}{r^2}$, the maximum of V_{null} occurs at $V'_{\text{null}} = 0$ leading to

$$2f(r_c) - r_c f'(r_c) = 0. \tag{24}$$

Hence the maximum of V_{scalar} and the location of the maximum of the null geodesics coincide at $r_m = r_c$. Cardoso *et al.* [36] presented the QNM frequencies in the eikonal limit as

$$\omega_{\text{QNM}} = \Omega_c l - i\left(n + \frac{1}{2}\right)|\lambda|. \tag{25}$$

Here, Ω_c is the coordinate angular velocity given as

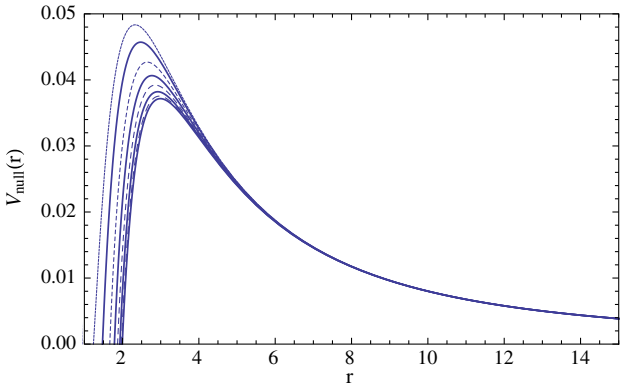

FIG. 16 (color online). The graph shows the relation of V_{null} with r for various values of the magnetic charge q. Here, $M = 1$ and $L = 1$. When q increases, V_{null} increases.

$$\Omega_c = \frac{\dot{\phi}}{\dot{t}}, \tag{26}$$

and λ is the Lyapunov exponent which is interpreted as the decay rate of the unstable circular null geodesics. The derivation of the above results is clearly given in Cardoso *et al.* [36]. For the Bardeen black hole, Ω_c and λ are given as

$$\Omega_c = \frac{\phi(r_c)}{\dot{t}(r_c)} = \sqrt{\frac{f(r_c)}{r_c^2}} = \sqrt{\frac{(r_c^2+q^2)^{3/2} - 2Mr_c^2}{r_c^2(r_c^2+q^2)^{3/2}}}, \tag{27}$$

$$\lambda = \sqrt{\frac{-V''_{\text{null}}(r_c)}{2\dot{t}(r_c)^2}} = \sqrt{\frac{-V''_{\text{null}}(r_c) r_c^2 f(r_c)}{2L^2}}. \tag{28}$$

From the values of Ω_c and λ, one can extract the real and the imaginary part of ω from Eq. (25) easily. In Figs. 17 and 18, Ω and λ are given for the Bardeen black hole. One can conclude that the behavior is very similar when ω was computed using the WKB approach in Sec. IV.

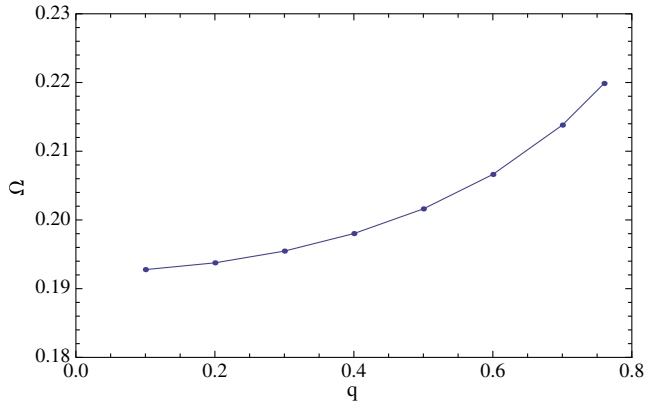

FIG. 17 (color online). The graph shows Ω_c as a function of q. Here, $M = 1$ and $L = 1$.

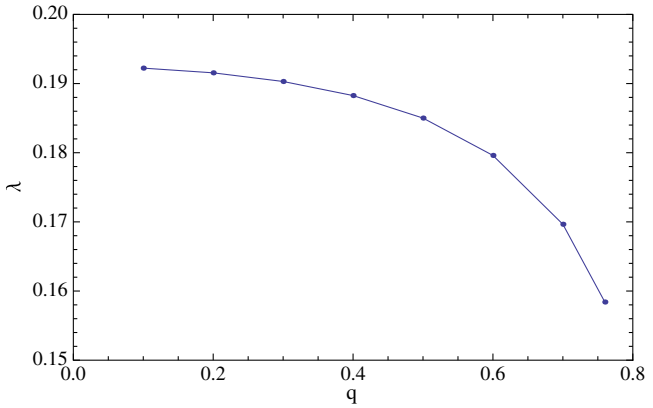

FIG. 18 (color online). The graph shows the Lyapunov exponent λ as a function of q. Here, $M = 1$ and $L = 1$.

One can compare the ω in the eikonal limit for the Reissner-Nordstrom black hole with the Bardeen black hole. First let us compute the r_c for the maximum of the effective potential for the photons of the Reissner-Nordstrom black hole as

$$r_c = \frac{1}{2}\left(3M + \sqrt{9M^2 - 8Q^2}\right). \tag{29}$$

Hence, λ_{RN} and Ω_{RN} can be computed with the Eqs. (27) and (28) with the corresponding metric function $f_{\text{RN}}(r)$. In Figs. 19 and 20 λ_{RN} and Ω_{RN} are plotted. Note that λ_{RN} has a maximum at $q = 0.7M$. For the Reissner-Nordstrom black hole, the oscillation frequency, ω_R, increases with the charge q. The damping rate, ω_I, increases and reaches a maximum at $q = 0.7M$ to decrease rapidly to zero at $M = q$. Ferrari and Mashhoon [38] presented QNM's of the Reissner-Nordstrom black hole. In that paper, the QNM's were presented in the eikonal limit ($l \gg 1$) and showed similar behavior. We like to note that the Lyapunov coefficients for the Reissner-Nordstrom black hole has been studied in detail in a recent paper by Pradhan [42].

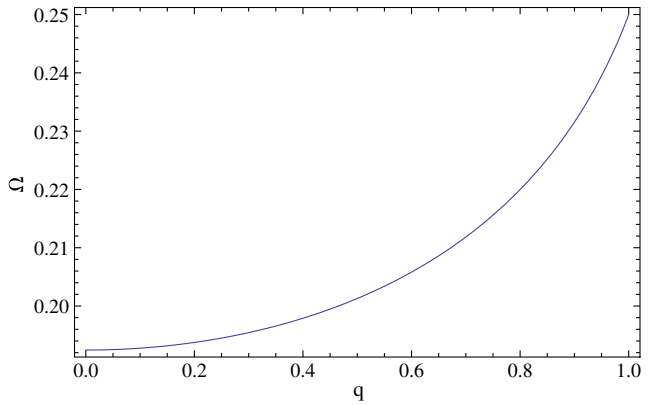

FIG. 19 (color online). The graph shows Ω_c as a function of q for the Reissner-Nordstrom black hole. Here, $M = 1$ and $L = 1$.

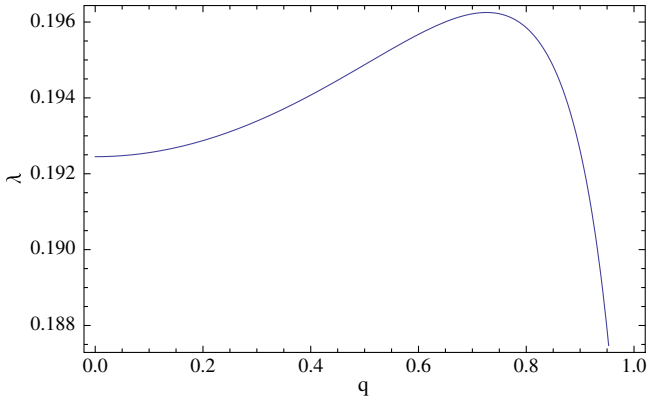

FIG. 20 (color online). The graph shows the Lyapunov exponent λ as a function of q for the Reissner-Nordstrom black hole. Here, $M = 1$ and $L = 1$.

B. On the expansion method to compute the QNM's at the eikonal limit

Dolan and Ottewill [43] developed an expansion method to compute QNM's at the eikonal limit to higher orders. Here, the basis for their approach is basically the same as given in Sec. VA where the null geodesics and the unstable circular orbits are the key to the computation. Other references where this method is applied are given in Refs. [39,44,45].

In this approach, the QNM's were expanded in inverse powers of $L = l + 1/2$. Let us first outline the formalism so that later we can apply it to the Bardeen black hole. We shall start with the master equation for the scalar perturbation given in Eq. (16),

$$\frac{d^2\xi(r)}{dr_*^2} + (\omega^2 - V_{\text{scalar}}(r_*))\xi(r) = 0, \tag{30}$$

where

$$V_{\text{scalar}}(r) = \frac{l(l+1)f(r)}{r^2} + \frac{f(r)f'(r)}{r}. \tag{31}$$

Now, redefine $\xi(r)$ as

$$\xi(r) = \exp^{(\int \frac{\alpha(r)}{f(r)} dr)}. \tag{32}$$

Here,

$$\alpha(r) = ib_c k_c(r)\omega. \tag{33}$$

The parameter b is called the ''impact parameter'' given by L/E and b_c is the value at $r = r_c$ which is the radius of the unstable circular orbit. L and E of the null geodesics are conserved quantities of the orbits given by

$$L = r^2\phi; \qquad E = f(r)t. \tag{34}$$

More information about the geodesics are given in Refs. [10,43] if one needs more details of the origin of these quantities.

Now, to define what $k_c(r)$ is, a new function $k^2(r, b)$ is defined as

$$k^2(r, b) = \frac{1}{b^2} - \frac{f(r)}{r^2}. \tag{35}$$

The origin of the function is in the equation for null geodesics given in Eq. (20) which also could be written as

$$\left(\frac{dr}{d\phi}\right)^2 \frac{1}{r^2} = \frac{1}{b^2} - \frac{f(r)}{r^2}. \tag{36}$$

In Dolan and Ottewill's paper [43], the assumption is made that there exists a critical impact parameter b_c, such that $k^2(r, b_c)$ has degenerated roots. Since at $r = r_c$, $dr/d\phi = 0$, this leads to

$$k^2(r_c, b_c) = 0; \qquad \left.\frac{\partial k^2(r, b_c)}{\partial r}\right|_{r=rc} = 0. \tag{37}$$

If the assumption is made that the repeated root is a double root, a new function $k_c(r)$ is defined as

$$k_c(r) = \text{Sign}(r - r_c)\sqrt{k^2(r, b_c)} = (r - r_c)K(r). \tag{38}$$

Here, $K(r)$ becomes

$$K(r) = \sqrt{\frac{k^2(r, b_c)}{(r - r_c)^2}}. \tag{39}$$

Hence, the function $k_c(r)$ is positive for $r > r_c$ and negative for $r < r_c$. If just $\sqrt{k^2(r, b_c)}$ is considered to be $k_c(r)$, then it would have lead to a function which is not differentiable at $r = r_c$. On the other hand, the definition given in Eq. (38) leads to a smooth function at $r = r_c$. To clarify these issues, we have plotted the graphs $k^2(r, b_c)$, $\sqrt{k^2(r, b_c)}$, $k_c(r)$ and $dk_c(r)/dr$ in Figs. 21 and 22.

Now that $k_c(r)$ is well established, on can substitute $\xi(r)$ into Eq. (30) which simplifies to be

$$\frac{d}{dr}\left(f(r)\frac{dv(r)}{dr}\right) + 2\alpha(r)\frac{df(r)}{dr} + (\omega^2 + \alpha(r)^2 - V_{\text{scalar}}(r) + f(r)\alpha'(r))\frac{v(r)}{f(r)} = 0. \tag{40}$$

Following the approach in Ref. [43], ω and $v(r)$ are expanded in inverse powers of L as

$$\omega_{n=0} = La_{-1} + a_0 + L^{-1}a_1 + L^{-2}a_2 + \ldots., \tag{41}$$

and

$$v_{n=0} = \exp(S_0(r) + L^{-1}S_1(r) + L^{-2}S_2(r) + \ldots.), \tag{42}$$

Note that in this paper, we are only interested in the fundamental modes corresponding to $n = 0$. The expansion could be done for higher modes with $n > 0$ as given in Ref. [43]. Now, the ω and $v(r)$ are substituted to Eq. (40) and similar powers of L are collected together as

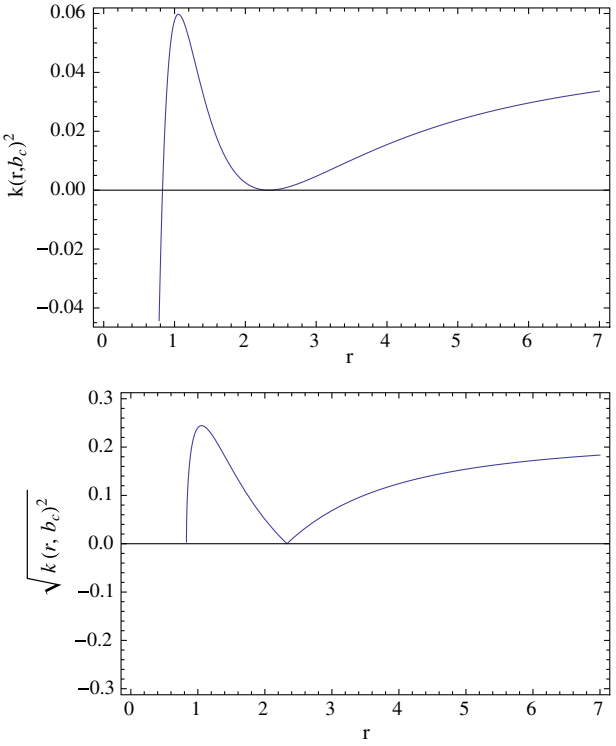

FIG. 21 (color online). The behavior of $k(r, b_c)$ and $\sqrt{k(r, b_c)^2}$ with r. Here, $M = 1$, $q = 0.76$, $r_c = 2.3299$ and $b_c = 4.5484$.

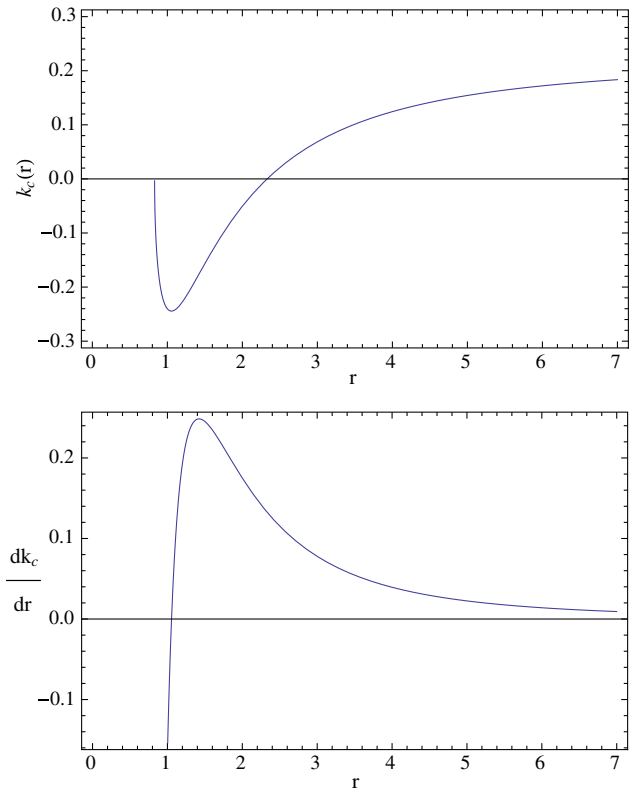

FIG. 22 (color online). The behavior of $k_c(r)$ and $\frac{dk_c(r)}{dr}$ with r. Here, $M = 1$, $q = 0.76$, $r_c = 2.3299$ and $b_c = 4.5484$.

$$L^2\colon\ a_1 = \sqrt{\frac{f(r_c)}{r_c^2}} = \frac{1}{b_c}, \tag{43}$$

$$L^1\colon\ \frac{2a_{-1}a_0}{f(r)} - \frac{2b_c^2k_c(r)^2a_{-1}a_0}{f(r)} + ib_ca_{-1}k_c'(r) + 2ib_ck_c(r)a_{-1}S_0'(r) = 0, \tag{44}$$

$$L^2\colon\ \left(\frac{1}{4r^2} - \frac{f'(r)}{r}\right) + (a_0^2 + 2a_{-1}a_1)\frac{(1 - b_c^2k_c(r)^2)}{f(r)} + (a_0S_0'(r) + a_{-1}S_1'(r))(2ib_ck_c(r)) + ia_0b_ck_c'(r) + f'(r)S_0'(r) + f(r)(S_0'(r)^2 + S_0''(r)) = 0. \tag{45}$$

Here $0000'$ denotes differentiation with respect to r. The coefficients a_i are found by imposing continuity condition at $r = r_c$. Once a_i are found, $S_i'(r)$ could be found. For example, from L^2 terms, a_{-1} is evaluated at $r = r_c$ as

$$a_{-1} = \sqrt{\frac{f(r_c)}{r_c^2}}. \tag{46}$$

Note that this is same as Ω_c computed in Eq. (27).

From L^2 term, a_0 is evaluated at $r = r_c$ as

$$a_0 = \frac{-ib_c}{2}f(r_c)k_c'(r_c). \tag{47}$$

By substituting a_0 and a_{-1} back into Eq. (44), one obtains $S_0'(r)$. One can differentiate $S_0'(r)$ to obtain $S_0''(r)$ and substitute to Eq. (45). Then, a_1 can be evaluated $r = r_c$. This process can be continued to find all a_i values and all $S_i'(r)$ functions. In this paper, we will only compute a_{-1}, a_0 and a_1 for the Bardeen black hole. We have chosen, $M = 1$ and $q = 0.76$ leading to $r_c = 2.3299$ and $b_c = 4.5484$. By the expansion method, the following a_i values are computed:

$$a_{-1} = 0.219858; \qquad a_0 = -0.0792063i; \qquad a_1 = 0.00499392. \tag{48}$$

Finally, $\omega_{n=0}$ in powers of L is written as

$$\omega_{n=0} = 0.219858L - 0.0792063i + 0.00499392L^{-1}. \tag{49}$$

VI. MASSIVE SCALAR PERTURBATIONS

In this section, we will address how the massive scalar field decays. For the Schwarzschild black hole, it has been observed that the massive modes decay slower than the massless field [46,47]. Hence it is interesting to see if such behavior is possible in the Bardeen black hole, leading to long-lived modes.

Let us first present the equation for a massive scalar field in curved space-time as

$$\nabla^2 \Phi - m^2 \Phi = 0. \quad (50)$$

Using the ansatz similar to Eq. (15), one obtain the modified potential as

$$V_{\text{massive}}(r) = \frac{l(l+1)f(r)}{r^2} + \frac{f(r)f'(r)}{r} + m^2 f(r). \quad (51)$$

The effective potential V_{massive} is plotted in Fig. 23 for varying values of the mass m of the scalar field.

The QNM's for the massive scalar field decay is computed using the WKB approximation discussed in Sec. IV. They are given in Figs. 24 and 25.

m	ω_R (n = 0)	ω_I (n = 1)	ω_R (n = 1)	ω_I (n = 1)
0	0.551623	0.0796005	0.534227	**
0.1	0.553910	0.0791170	0.536006	0.282895
0.2	0.560821	0.0776240	0.541304	0.280290
0.3	0.572499	0.0749856	0.550006	0.279202
0.4	0.589201	0.0709443	0.561865	0.278647
0.5	0.611305	0.0650541	0.576393	0.278327
0.6	0.639305	0.0565300	0.590768	0.278125
0.64	0.652259	0.0520869	0.586619	0.176782
0.67	0.662598	0.0482116	0.542126	0.162060
0.69	0.669602	0.0452134	0.377631	0.149858

From Fig. 24, the real part of the lowest QNM frequency increases with mass of the field. However, for the first overtone ($n = 1$), the real part of QNM reaches a maximum and decreases rapidly with the mass of the field. Ohashi and Sakagami did an analysis on the QNM's for the Reissner-Nordstrom black hole with the massive scalar field in Ref. [48]. The real part of the ω shows similar behavior as for the ω_R for $n = 0$ for the Bardeen black hole. The imaginary part of the ω decreases with the mass for the Bardeen black hole for both values of n. This is similar to the behavior shown for ω_I of the Reissner-Nordstrom black hole [48].

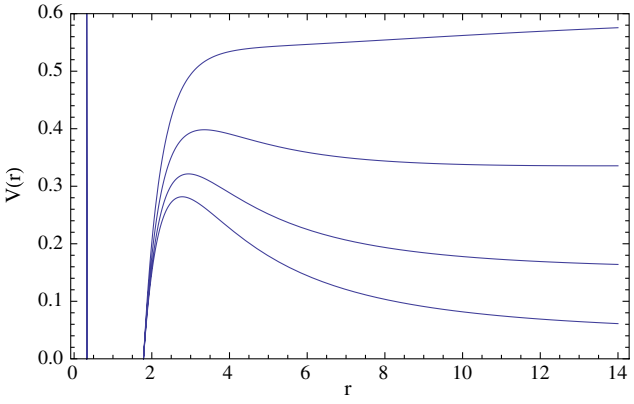

FIG. 23 (color online). The behavior of V_{massive} with the mass m of the scalar field. Here $M = 1$, $q = 0.5$, and $l = 2$. When the mass decreases, the height of the effective potential also decreases.

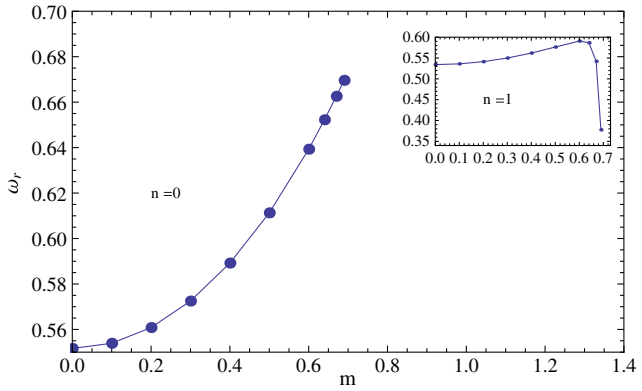

FIG. 24 (color online). The behavior of Re ω with the mass of the scalar field m for $M = 1$, $q = 0.76$, and $l = 1$. Plots for $n = 0$ and $n = 1$ are given.

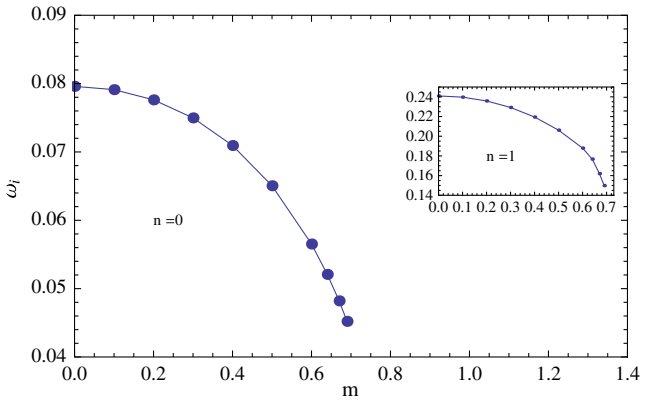

FIG. 25 (color online). The behavior of Im ω with the mass of the scalar field m for $M = 1$, $q = 0.76$, and $l = 1$. Plots for $n = 0$ and $n = 1$ are given.

VII. SUMMARY

We have studied the scalar perturbations of the Bardeen black hole. The quasinormal mode spectrum of the massless scalar field is computed for various values of the charge q, mass M, and the spherical index l. The QNM spectrum is also computed for the Reissner-Nordstrom black hole by varying the charge along with the Bardeen black hole and comparing the behavior.

We have also applied the unstable null geodesics of the black hole to compute the QNM frequencies in the eikonal limit ($l \gg 1$). Once again, a comparison is done with the QNM frequencies of the Reissner-Nordstrom black hole in the eikonal limit. We have also introduced the expansion

method to compute ω in inverse powers of L following the approach by Ref. [43].

Finally, the QNM frequency spectrum is computed for the massive scalar field. A discussion is also presented comparing the spectrum to the massive modes of the Reissner-Nordstrom black hole.

VIII. DIRECTIONS FOR FURTHER STUDY

There are several avenues to proceed from here to extend this work. For the Reissner-Nordstrom black hole, in the eikonal limit ($l \gg 1$), the effective potentials for scalar, Dirac and gravitational perturbations are approximately the same. This is clearly presented in the paper by Ferrari and Mashhoon [38]. It would be interesting to do the analysis on gravitational perturbations and Dirac perturbations of the Bardeen black hole to see if similar behavior persists.

Highly damped asymptotic QNM's of the black hole is not studied in this paper. As mentioned in the introduction, that is a very active area of research on QNM's. It would be interesting to extend this work to study ω for large n values. Motl and Neitzke [49], did an analytical study to compute the asymptotic QNM's for the Reissner-Nordstrom black hole. It would be interesting to compare the asymptotic values of the Bardeen black hole with such values to understand how the nonlinear nature effects the physical properties of the black holes.

It would be interesting to compute higher-order expansions of ω in the eikonal limit using the approach in Ref. [43].

An extension of the Bardeen blackhole with a nonlinear electromagnetic source presented by Ayón-Beato and García [5] has been studied by Nomura and Tamaki [50]. The metric of this black hole is given by

$$ds^2 = -f(r)dt^2 + f(r)^{-1}dr^2 + r^2(d\theta^2 + \sin^2(\theta)d\varphi^2), \tag{52}$$

where

$$f(r) = 1 - \frac{2Mr^2}{(r^2+q^2)^{3/2}} + \frac{q^2r^2}{(r^2+q^2)^2}. \tag{53}$$

Nomura and Tamaki concluded that the QNM frequencies become pure imaginary when $n \longrightarrow \infty$. It would be interesting to see if such behavior persists in all nonlinear sources such as the one presented in this paper.

With regard to the QNM's for the massive scalar field, it would be interesting to do an analytical study if possible, to find a bound on the mass m when ω_I becomes zero.

ACKNOWLEDGMENTS

S. F. like to thank R. A. Konoplya for providing the WKB approximation.

[1] J. Bardeen, in Proceedings of GR5, Tiflis, U.S.S.R. (Unpublished).
[2] A. Borde, Phys. Rev. D **50**, 3692 (1994).
[3] A. Borde, Phys. Rev. D **55**, 7615 (1997).
[4] E. Ayón-Beato and A. García, Phys. Lett. B **493**, 149 (2000).
[5] E. Ayón-Beato and A. García, Phys. Lett. B **464**, 25 (1999).
[6] E. Ayón-Beato and A. García, Gen. Relativ. Gravit. **31**, 629 (1999).
[7] E. Ayón-Beato and A. García, Phys. Lett. B **493**, 149 (2000).
[8] E. Ayón-Beato and A. García, Gen. Relativ. Gravit. **37**, 635 (2005).
[9] E. F. Eiroa and C. M. Sendra, Classical Quantum Gravity **28**, 085008 (2011).
[10] S. Zhou, J. Chen, and Y. Wang, arXiv:1112.5909.
[11] C. Moreno and O. Sarbach, Phys. Rev. D **67**, 024028 (2003).
[12] M. Sharif and W. Javed, J. Korean Phys. Soc. **57**, 217 (2010).
[13] G. T. Horowitz and V. E. Hubeny, Phys. Rev. D **62**, 024027 (2000).
[14] S. Hod, Phys. Rev. Lett. **81**, 4293 (1998).
[15] R. A. Konoplya and A. Zhidenko, Rev. Mod. Phys. **83**, 793 (2011).
[16] B. Chen and J. Zhang, Phys. Rev. D **84**, 124039 (2011).
[17] Y. Kim, Y. S. Myung, and Y. Park, arXiv:1205.3701.
[18] I. Z. Stefanov, S. S. Yazadjiev, and G. G. Gyulchev, Phys. Rev. Lett. **104**, 251103 (2010).
[19] C. Chirenti, A. Saa, and J. Skakala, arXiv:1206.0037.
[20] S. Chandrasekhar, *The Mathematical Theory of Black Holes* (Oxford University Press, New York, 1992).
[21] D. Birmingham, Phys. Rev. D **64**, 064024 (2001).
[22] S. Fernando, Phys. Rev. D **77**, 124005 (2008).
[23] S. Fernando, Gen. Relativ. Gravit. **37**, 585 (2005).
[24] Y. S. Myung and T. Moon, arXiv:1204.2116.
[25] R. Li, Int. J. Mod. Phys. D **21**, 1250014 (2012).
[26] R. Cordera, A. López-Ortega, and I. Vega-Acevedo, Gen. Relativ. Gravit. **44**, 917 (2012).
[27] A. Nunez and A. Starinets, Phys. Rev. D **67**, 124013 (2003).
[28] S. Iyer and C. M. Will, Phys. Rev. D **35**, 3621 (1987).
[29] R. A. Konoplya, Phys. Rev. D **68**, 024018 (2003).
[30] S. Fernando and K. Arnold, Gen. Relativ. Gravit. **37**, 585 (2005).
[31] S. Fernando and C. Holbrook, Int. J. Theor. Phys. **45**, 1630 (2006).
[32] S. Fernando, Int. J. Mod. Phys. A **25**, 669 (2010).
[33] E. W. Leaver, Phys. Rev. D **41**, 2986 (1990).
[34] N. Anderson, Proc. R. Soc. B **442**, 427 (1993).

[35] V. P. Frolov and I. D. Novikov, *Black hole physics* (Kluwer Academic Publishers, 1998).
[36] V. Cardoso, A. S. Miranda, E. Berti, H. Witeck, and V. T. Zanchin, Phys. Rev. D **79**, 064016 (2009).
[37] B. Mashhoon, Phys. Rev. D **31**, 290 (1985).
[38] V. Ferrari and B. Mashhoon, Phys. Rev. D **30**, 295 (1984).
[39] S. R. Dolan, Phys. Rev. D **82**, 104003 (2010).
[40] S. Hod, Phys. Rev. D **80**, 064004 (2009).
[41] J. Morgan, V. Cardoso, A. S. Miranda, C. Molina, and V. T. Zanchin, Phys. Rev. D **80**, 024024 (2009).
[42] P. Pradhan, arXiv:1205.5656.
[43] S. R. Dolan and A. C. Ottewill, Classical Quantum Gravity **26**, 225003 (2009).
[44] S. R. Dolan and A. C. Ottewill, Phys. Rev. D **84**, 104002 (2011).
[45] S. R. Dolan, L. A. Oliveira, and C. B. Crispino, Phys. Rev. D **85**, 044031 (2012).
[46] L. M. Burko and G. Khanna, Phys. Rev. D **70**, 044018 (2004).
[47] R. A. Konoplya and A. V. Zhidenko, Phys. Rev. D **71**, 047502 (2005).
[48] A. Ohashi and M. Sakagami, Classical Quantum Gravity **21**, 3973 (2004).
[49] L. Motl and A. Neitzke, Adv. Theor. Math. Phys. **7**, 307 (2003).
[50] H. Nomura and T. Tamaki, Phys. Rev. D **71**, 124033 (2005).